Measuring Soil Moisture with Imaging Radars

Pascale C. Dubois(*), Jakob van Zyl(*) and Ted Engman (**)

Abstract—An empirical algorithm for the retrieval of soil moisture content and surface Root Mean Square (RMS) height from remote.ly sensed radar data was developed using scatterometer data. The algorithm is optimized for bare surfaces and requires two co-polarized channels at a frequency between 1.5 GHz and 11 GHz. It gives best results for $kh \leq 2.5$, $\mu_v \leq 35\%$ and $\theta \geq 30°$

Omitting the usually weaker hv-polarized returns makes the algorithm less sensitive to system cross-talk and system noise, simplify the calibration process and adds robustness to the algorithm in the presence of vegetation. However, inversion results indicate that significant amounts of vegetation (NDVI > 0.4) cause the algorithm to underestimate soil moisture and overestimate RMS height. A simple criteria based on the $\sigma^0_{hv}/\sigma^0_{vv}$ ratio is developed to select the areas where the inversion is not impaired by the vegetation.

The inversion accuracy is assessed on the original scatterometer data sets but also on several SAR data sets by comparing the derived soil moisture values with *in-situ* measurements collected over a variety of scenes between 1989 and 1994. Both spaceborne (SIR-C) and airborne (AIRSAR) data are used in the test. Over this large sample of conditions, the RMS error in the soil moisture estimate is found to be less than 3.5% soil moisture.

(*): Jet Propulsion Laboratory, California Institute of Technology
4800 Oak Grove Drive, Pasadena CA 91009
(**) NASA Goddard Space Flight Center
Code 974, Greenbelt,MlJ20771
E-mail: pascale@blacks.jpl.nasa.gov Ph: (818) 3540497 Fx: (818) 3936943

1. INTRODUCTION

A key element to understanding the nature of global change is the ability to model the two-way interaction between land and atmosphere. Perhaps the most important role that the land surface component performs is the partitioning of incoming radiative energy into sensible and latent heat fluxes. There have been a number of modeling studies that have demonstrated the sensitivity of soil moisture anomalies to climate [1 ,2]. Shukla (personal communication) for instance, reports that soil moisture is the second most important forcing function, second only to the sea surface temperature in the mid-latitudes, and it becomes the most important forcing function in the summer months.

The role of soil moisture is equally important at smaller scales. Recent studies with mesoscale atmospheric models have similarly demonstrated a sensitivity to spatial gradients of soil moisture. For example, Fast et al. [3] has shown that moisture gradients can induce thermally induced circulations similar to sca breezes. Chang and Wetzel[4] have concluded that the spatial variations of vegetation and soil moisture affect the surface baroclinic structures through differential heating which in turn indicate the location and intensity of surface dynamic and thermodynamic discontinuities necessary to develop severe storms. In yet another study, Lanicci et al [5] have shown that dry soil conditions over the southern Great Plains can dynamically interact to alter pre-storm conditions and subsequent convective rainfall patterns. More recently, Betts et al. [6] demonstrated that the initialization of the Global Climate Model Weather Forecast (GCM WF) weather predictions with current soil moisture values can lead to improved rainfall predictions.

In addition to the role of soil moisture in the interactions between the land surface and the atmosphere, soil moisture is a storage of water timewise between rainfall and evaporation that acts as a regulator to one of the more fundamental hydrologic processes, infiltration and runoff production from rainfall and which must be accounted for in any water and energy balances.

Active microwave data has been shown to depend on several natural surface parameters such as dielectric constant [7,8] and surface roughness [9]. The dielectric constant is highly dependent on soil moisture due to the large difference in dielectric constant between dry soil (typical dielectric constants of 2-3) and water (dielectric constant of approximately 80). Estimating soil moisture from active microwave data has received much attention lately, The feasibility of the inversion has been demonstrated

in [10] for scatterometer data. Because of characteristic high resolution combined with potential global coverage, spaceborne SAR can provide a unique perspective on the spatial and temporal variation in soil moisture both at a relatively high resolution (e.g., gradient of moisture within a field or along the slope of a hill) and at a global scale (features of the order of 10 km). Furthermore, the increased number of SAR systems (AIRSAR, E-SAR, ERS- 1, JERS-1 and SIR-C) together with their good calibration performance has made SAR data more readily available for the quantitative retrieval of soil moist ure.

Theoretical models can predict the general trend of radar backscatter in response to changes in roughness or soil moisture reasonably well; however, they can rarely be used to invert data measured from natural surfaces, mainly because of their complexity or the restrictive assumptions made when deriving them.

To circumvent the difficulties in applying theoretical models to data measured from natural surfaces, an empirical model was developed to infer soil moisture and surface roughness from radar data. In developing this algorithm, several goals were set:
1) The algorithm should be applicable to as wide a data set as possible
2) The calibration requirements on the data created by the algorithm should be practical.
3) The algorithm should be applicable in the presence of low vegetation.

To address the first (and to some extend the second) goal, we developed the algorithm using ground based scatterometer data from the LCX POLARSCAT [11], and the RASAM systems [12]. The variety of sources of training data, with their accompanying differences in calibration accuracies, adds robustness to the algorithm and makes it more applicable to other data sets. The second and third goals dictated the use of only co-polarized backscatter coefficients. These signals are less sensitive to system noise and cross-talk than the weaker cross-polarized returns. Also, co-polarized returns are easily calibrated using a variety of calibration targets and devices; something that is not generally true for cross-polarized returns. Finally, the co-polarized returns are affected less by the presence of the vegetation than the cross-polarized terms, providing increased robustness.

The accuracy of the inversion technique is assessed for both scatterometer data and Synthetic Aperture Radar (S AR) (e.g., AIRSAR and SIR-C) data by comparing soil moisture obtained with the inversion technique to *in situ* measurements over bare surfaces. In the case of the imaging radar data, the algorithm was found to underestimate

the soil moisture in the presence of vegetation. To circumvent this problem, a SAR vegetation index is used to automatically eliminate the heavily vegetated areas where the inversion results are not reliable. The SAR vegetation index is shown to correlate positively to the well-known Normalized Difference Vegetation Index (NDVI).

II. EXPERIMENTAL DATA AND MODEL DESCRIPTION

Two sources of experimental data were used in the derivation of the empirical model. The university of Michigan's LCX POLARSCAT is a truck-mounted network-analyzer-based scatterometer operating at three frequencies 1.25,4.75 and 9.5 GHz. A complete description of the instrument can be found in [11], The POLARSCAT data set [10] used in this study includes the co- and cross-polarized (hh, vv and hv) backscatters for four surfaces. At least ten roughness profiles were acquired over each of the four surfaces by using a laser profilometer mounted on an X-Y table with a 2.5 mm horizontal resolution and a 2 mm vertical accuracy over a length of 1 meter. Using these surface profiles, a RMS height was computed for each of the four surfaces. The university of Michigan team also measured the dielectric constant of the soil surfaces using a C-band field-portable dielectric probe (PDP) [13] at the top surface and at a depth of 4 cm. The dielectric constant (E) was converted to volumetric soil moisture (μ_v) through a set of empirical curves [14]. An average value representing, the soil moisture for the O-4 cm layer was computed and the soil density was determined from soil samples with known volumes. The data set consists of measurements over four surfaces with RMS height varying from 0.32 cm to 3.02 cm. The resulting electromagnetic roughnesses cover a wide range of value from kh = 0.1 to kh = 6.01 (where $k = 2\pi/\lambda$ is the wave number, λ is the wavelength and h is the RMS height). For each surface, two wetness states were studied: a relatively dry condition with volumetric soil moisture ranging from 0.14 to 0.19 and a relative] y wet condition with volumetric soil moisture ranging from .20 to .31. The scatterometer measurements were acquired every 10° between 10° and 70°. Table 1 summarizes the ground truth for the POLARSCAT data.

The university of Berne's RASAM is a truck-mounted radiometer-scatterometer with the scatterometer system operating at six frequencies between 2.5 GHz and 11 GHz. A complete description of the instrument can be found in [15]. The RASAM data set [12] includes measurements of the hh, vv, hv and vh-polarized backscattering coefficients over a variety of surfaces. Only bare surfaces were selected for this study. Among bare surfaces, furrowed fields were excluded to avoid the significant enhanced scattering occurring when the furrows are almost perpendicular to the plane of the incident

electromagnetic wave [16, 17] (the angle between the. radar incident plane and the furrows was not available in the report). For each field, several surface profiles were acquired with a laser profilometer [18] with a horizontal spacing of 0.5 mm and a vertical accuracy of 0.1 mm. A surface RMS height is derived from these profiles after proper detrending. Furthermore, gravimetric soil samples and soil density measurements were collected to characterize the volumetric soil moisture corresponding to the O-4 cm top soil layer. 'I'he gravimetric sand fraction and clay fraction were also determined. The selected RASAM data set consists of measurements over eight surfaces with RMS height varying from 0.57 cm to 1.12 cm. The resulting electromagnetic rough nesses cover values ranging from kh = 0.3 to kh = 2.6. The volumetric soil moist ure ranges from 0.17 to 0.28. The backscatter measurements were made every 10° between 30° and 60°. Table 2 summarizes the bare surface characteristics.

Using these two data sets, an empirical model was derived to describe the co-polarized backscatter coefficients of bare surfaces as a function of surface roughness, dielectric constant, incidence angle and frequency. The dielectric constant is the parameter sensitive to volumetric soil moisture, The hh-polarized and vv-polarized backscattering coefficients σ^o_{hh} and σ^o_{vv} were empirically found to follow these two equations:

$$\sigma^0_{hh} = {}^{,\,0\text{-}2.75}\,\frac{\cos^{1.5}\theta}{\sin^5\theta}\,100\text{"}28\text{cuno}(\sim\sim\sin\sim)142{,}07$$

$$\sigma^0_{vv} = 10^{-2.5}\,\frac{\cos^3\theta}{\sin^3\theta}\,10^{0.46\varepsilon\tan\theta}(kh\sin\theta)^{1.1}\lambda^{0.7} \qquad (1)$$

where θ is the incidence angle, ε is the real part of the dielectric constant, *h is* the RMS height of the surface, *k is* the wave number and λ is the wavelength in cm. These two relations are valid for frequencies varying between 1.5 and 11GHz, for surfaces with roughness ranging from 0.3 to 3 cm RMS height (the range of the training data set) and for incidence angle between 30° and 65°.

The general backscatter behavior with roughness is similar to the trend predicted by the small perturbation model and the physical optics model [19]. The backscatters decrease with increasing incidence angle and with decreasing roughness. The small perturbation model predicts the following hh - and vv-polarized backscatter:

$$\sigma^0_{hh} = 8k^4h^2\,\cos^4\theta\,W(2k\sin\theta)\left|\alpha_{hh}(\theta)\right|^2 \qquad (2)$$

$$\sigma_{vv}^0 = 8k^4h^2\cos^4\theta\, W(2k\sin\theta)\left|\alpha_{vv}(\theta)\right|^2$$

with

$$\alpha_{hh}(\theta) = \frac{(\varepsilon-1)}{\left(\cos\theta+\sqrt{\varepsilon-\sin^2\theta}\right)^2} \qquad (3)$$

$$\alpha_{vv}(\mathrm{e}) = \frac{(\varepsilon - 1)(8(1+\sin 20) - \sin 20)}{\left(\cos\theta+\sqrt{\varepsilon-\sin^2\theta}\right)^2}$$

where *W is* the surface roughness spectrum.

In the case of an exponential correlation function, the roughness spectrum *W* takes the following form:

$$W(2k\sin\theta) = \frac{1}{271}\frac{l^2}{\left(1+4k^2\sin^2\theta\, l^2\right)^{1.5}} \qquad (5)$$

where l is the correlation length of the surface.

When $2k\sin\theta >> 1$, (5) can be written as:

$$W(2k\sin\theta) \cong \frac{1}{2\pi}\frac{1}{8k^3\sin^3\theta} \qquad (6)$$

It results that:

$$\sigma_{hh}^0 \cong C_1\frac{2h}{l}\frac{\cos^4\theta}{\sin^4\theta}\left|\alpha_{hh}(\theta)\right|^2 kh\sin\theta$$

$$\sigma_{vv}^0 \cong C_2\frac{2h}{l}\frac{\cos^4\theta}{\sin^4\theta}\left|\alpha_{vv}(\theta)\right|^2 kh\sin\theta \qquad (7)$$

where C_1 and C_2 are two constants.

In both the empirical model and the small perturbation model, the RMS height of the surface is introduced via the $kh\sin\theta$ factor which is the dimensionless form of the projected roughness on the wave incident plane. The power of this parameter in the empirical model (1.4 and 1.1 for respectively σ_{hh}^o and σ_{vv}^o) is close to the power 1 for both σ_{hh}^o and σ_{vv}^o in the case of the small perturbation model with an exponential correlation function.

Note that the model described in (1) does not follow the SPM model even in the case of very smooth surfaces: Our expressions in (1) do predict that as the roughness increases, the ratio $\sigma^0_{hh}/\sigma^0_{vv}$ will also increase due to the difference. in the power of $kh \sin\theta$ whereas the SPM model results in a $\sigma^0_{hh}/\sigma^0_{vv}$ ratio that does not depend on the roughness. This increasing trend is to be expected considering that very rough surfaces have the same backscatter at hh and vv-polarizations according to the geometrical optics model. However, we note that for very large values of $kh \sin\theta$, σ^o_{hh} will become larger than σ^o_{vv}, contrary to what is predicted by most theoretical models (except Physical Optics model) and contrary to what has been observed on SAR data. Restricting the validity of the model to $kh \leq 2.5$ and $\theta \geq 30°$ will ensure that (he $\sigma^0_{hh}/\sigma^0_{vv}$ ratio is always less than 1 in agreement to what is observed in the data. Until more data becomes available, we are unable to refine (1) to describe the backscatter of rougher surfaces at an incidence angle smaller than 30°. We note, however that the natural surfaces that we appl y the algorithm to, rarely exceed $kh = 2.5$ (corresponding for 1.-band to a RMS height of 10 cm)

In (1), the backscatters as well as the $\sigma^0_{hh}/\sigma^0_{vv}$ decrease with increasing dielectric constant. Furthermore, because of the tan 0 multiplicative factor, the dielectric constant has a weaker effect at smaller incidence angles. These trends are qualitatively in agreement with both the small perturbation model and the physical optics model.

111. SCATTEROMETER RESULTS

From the σ^0_{hh} and σ^0_{vv} measurements and the empirical model described in (1), one can easily compute the relative dielectric constant of the soil ε, and the RMS height of the surface h. The conversion from dielectric constant to volumetric soil moisture is done using a set of empirical formulas [14] describing how the dielectric constant varies with soil texture. Figure 1 presents the values of soil moisture and surface roughness estimated from the backscatter values versus the *in-situ* measurements for the POLARSCAT data. Each point on the plot corresponds to one surface and one wetness condition where the soil moisture (RMS height) is the average soil moisture (RMS height) estimated over the different incidence angles and different frequencies. The straight diagonal line describes a perfect inversion algorithm where the estimated values match exactly the measured values. Deviations away from this line are errors. The RMS errors are 4.5% for the estimates of soil moisture and *0.34* cm for the estimate of the RMS height.

IV. EFFECTS OF VEGETATION

The accuracy of the inversion when applied to other datasets depends on two factors: 1) The presence of vegetation 2) the calibration of the radar system. These two effects are investigated in the following paragraphs.

The inversion method was derived from data collected over bare surfaces. It relies on the co-polarized channels and does not use the cross-polarized channels. This has several advantages. The first advantage is that the co-polarized channels can be calibrated directly with passive targets like corner reflectors, The cross-polarized channel calibration is usually derived from measurement of the co-polarized channels [20] and as a result is less accurate than the calibration on the co-polarized channels. The second advantage is the usually higher signal-to-noise ratio in the co-polarized channels than in the cross-polarized channels. Finally, vegetation is known to have a relative strong effect on the cross-polarized channel [21,22]. One of the main effects of vegetation is to introduce a volume scattering term in both the co- and the cross-polarized channels. This effect is relatively large for the cross-polarized channel. It can therefore be expected that an inversion algorithm relying on the co-polarized channels will be more robust to presence of vegetation than one relying on both the cross and the co-polarized channels. Nevertheless, for a significant amount of vegetation, the backscatter of the vegetated surface is higher than that of a bare surface and the $\sigma^0_{hh}/\sigma^0_{vv}$ ratio is closer to 1. The expressions in (1) predict that the higher backscatter caused by the vegetation can be interpreted as either an increase in roughness or an increase in dielectric constant. However, an increase in the dielectric constant would correspond to a decrease in the $\sigma^0_{hh}/\sigma^0_{vv}$ ratio whereas vegetation causes an increase in the co-polarized ratio. Therefore, the presence of vegetation will result in an overestimated surface roughness and an underestimated soil moisture.

Active microwave sensors have been shown to be a good discriminator for biomass [21], This capability can be used to select the areas with low vegetation cover where the inversion can be applied. In Figure 2, the L-band $\sigma^0_{hv}/\sigma^0_{vv}$ ratio image of data acquired over Chickasha, Oklahoma is presented together with a SPOT derived Normalized Difference Vegetation Index (NDVI) image [23,24] over the same area. Overall, a pixel-to-pixel comparison between the two indices provides the regression curve plotted in Figure 3. This curve shows that the L-band parameter does not have a good sensitivity to vegetation with NDVI below 0.2. This indicates that when the vegetation is very sparse, the scattering at L-band is dominated by interactions with the underlying surface and not

with the vegetation. The regression curve stops at NDVI 0.6 because few pixels in the SPOT image exceed 0.6. As expected, the correspondence between the two indices is noisy with a wide standard deviation (also displayed in Figure 3). Nevertheless, the curve indicates a definite correlation between the two indices confirming the potential of the $\sigma^0_{hv}/\sigma^0_{vv}$ ratio to be a good vegetation index.

The question is how to decide which level of the $\sigma^0_{hv}/\sigma^0_{vv}$ ratio above which the area vegetation cover is too thick for the inversion to apply. The inversion algorithm was tested over a scene for which the soil moisture was known to be uniformly saturated as the data were acquired following an intense rainy period. Blindly applying the algorithm to all pixels in the image indicated that for the vegetated areas in the image, the algorithm underestimated the moisture. Furthermore, the areas where the algorithm predicted drier conditions were well correlated with areas with high L-band $\sigma^0_{hv}/\sigma^0_{vv}$ ratio. We found that masking out the areas for which the L-band $\sigma^0_{hv}/\sigma^0_{vv}$ ratio is greater than -11 dB, results in a soil moisture image in which the algorithm estimates consistently wet conditions everywhere. No further tests could be done to validate this result over other scenes and different vegetation types by lack of ground truth. However, it is in agreement with other related studies. For bare surfaces, the $\sigma^0_{hv}/\sigma^0_{vv}$ ratio was shown to saturate at around -10 dB for surfaces with $kh > 3$ [10]. Therefore, if we mask areas with the ratio $\sigma^0_{hv}/\sigma^0_{vv}$ larger than -11 dB as too heavily vegetated for the algorithm to apply, it follows that few bare surfaces would be masked out and be mistaken for vegetated surfaces. Those bare surfaces that are mistaken as being too heavily vegetated will most likely be too rough (recall that we prefer to apply our algorithm to surfaces with $kh < 2.5$) to provide accurate results. As an aside, note that according to Figure 3, the $\sigma^0_{hv}/\sigma^0_{vv}$ ratio is only sensitive to vegetation for NDVI larger than 0.2. A ratio $\sigma^0_{hv}/\sigma^0_{vv}$ of -11 dB corresponds to an NDVI of 0.4 (see Figure 3). This again indicates that the co-polarized channels are less sensitive to vegetation than the cross polarized channels, and that the inversion could be applied to surfaces with NDVI as high as 0.4.

V. EFFECT OF CALIBRATION ERRORS

Two different calibration requirements on the radar system need to be considered: the absolute calibration and the relative calibration. An absolute calibration error can be modeled as a multiplicative factor affecting both σ^0_{hh} and σ^0_{vv}. A relative calibration error can be modeled as a multiplicative factor to be applied to $\sigma^0_{hh}/\sigma^0_{vv}$.

To assess the calibration requirements on the radar system, one may consider a surface with a known RMS height and soil moisture (dielectric constant). The corresponding σ^0_{hh} and σ^0_{vv} can then be computed using (1) and perturbed by the calibration errors as follows:

$$\hat{\sigma}^0_{hh} = C_a \sqrt{C_r}\, \sigma^0_{hh}$$
$$\hat{\sigma}^0_{vv} = C_a / \sqrt{C_r}\, \sigma^0_{vv} \qquad (8)$$

where C_a is the absolute calibration error and C, is the relative calibration error. The values of $\hat{\sigma}^0$ can be used to compute an estimate soil moisture and surface roughness to be compared with the original soil moisture and surface roughness.

Figure 4a and 4b represent respectively how the estimates of soil moisture μ_v (derived from $\hat{\sigma}^0_{hh}$ and $\hat{\sigma}^0_{vv}$) vary when an absolute (with C_r=0), relative (with C_a=0) calibration error is introduced for different incidence angles, These Figures show that the inversion is more robust to calibration errors at larger incidence angle: the error introduced by the same calibration error results in a larger error in the estimation of the soil moisture at 30° than at 60°. The error is also more sensitive to relative than absolute calibration. An error in the soil moisture estimation of 3.5% at 45° corresponds to a 0.5 dB error in the relative calibration or to a 2 dB absolute calibration error.

The fully-polarized JPL/NASA Airborne SAR system AIRSAR operates at C-, L- and P-bands [25]. The SIR-C SAR is a spaceborne imaging radar operating at C- and L-band with a full polarization option. Both systems are producing calibrated images as standard products, The absolute and relative calibration accuracy obtained for each sensor are listed in the Table 3 [26,27 ,28] For the SIR-C sensor, the evaluation of the calibration accuracy is still in progress and the pre-mission calibration requirements are listed in the table, although early results indicate that the requirements will be met by the data. The validity of these numbers covers all the scenes and it does not require the presence of in-scene calibration targets, The comparison of Figure 4 and Table 3 indicates that the calibration requirements dictated by the inversion for a 4% accuracy in soil moisture estimate are met by both the AIRSAR and the SIR-C sensor, except for the P-band AIRSAR data. It should therefore be possible to derive accurate soil moisture maps for the data provided operationally by these sensors,

V]. SAR DATA INVERSION

The inversion technique was applied to AIRSAR and SIR-C images. For both datasets, the images were first segmented into two classes according to the $\sigma^0_{hv}/\sigma^0_{vv}$ ratio. The inversion was applied to the class corresponding to the sparser vegetation cover, i.e., for which the $\sigma^0_{hv}/\sigma^0_{vv}$ ratio was less than -11 dB. The inversion was applied to the L-band data only. For sparsely vegetated fields, the vegetation is known to be more transparent at L-band than at C-band and P-band calibration is not quite good enough to provide reliable soil moisture maps.

The inversion technique was first applied to Washita'92 AIRSAR data. The Washita'92 [29] and Washita '94 are field campaigns designed to provide ground truth soil moisture data and the supporting hydrologic data for microwave remote sensing algorithm development and hydrologic studies with a focus on remotely sensed soil moisture. The USDA ARS Little Washita Watershed was selected for these efforts because of the extensive hydrologic research that has been conducted therein the past, and the ongoing hydrologic data collection efforts. The Little Washita Watershed is a 610 square km drainage basin situated in the southern part of the Great Plains in southwest Oklahoma. The climate is classified as moist and subhumid with an average annual rainfall of about 640 mm. During the field campaigns, extensive soil moisture measurements were taken, surface roughness data obtained, and vegetation cover was characterized and sampled. Washita'92 was a multisensory Aircraft Campaign (MAC) conducted from June 10 to June 18, 1992. The observations followed a period a heavy rain so that the conditions on June 10 were very wet with standing water and saturated soils fairly common. No further rain fell during the next nine days and we were able to follow a drying pattern. SAR data were collected with the JPL AIRSAR, flying on a DC-8 aircraft. Aircraft and extensive field data were collected each day during this period except for June 15 which was an aircraft crew rest day.

The area covered in Figure 5 is around 8 km by 10 km. It was imaged by the AIRSAR system on six different days between June 10 and June 18, 1992. The six L-band images were processed by the AIRSAR operational processor providing calibrated data sets. All the images, initially in slant range projection were transformed into a ground range projection [30] and the five successive data sets were registered to the June 10 data take [31] to allow an easy comparison. An L-band hh image is displayed at the lower right corner. The AGO02 bare field is outlined in the image. This field was extensively studied during the experiment. The six color images were obtained by

inverting the L-band data acquired on the corresponding days. The dielectric constant maps were translated into soil moisture maps using the Hallikainen empirical curves [14]. The black areas in the soil moisture maps indicate areas where the vegetation cover is too thick for the inversion to be reliable. The blue areas correspond to the wettest conditions, the yellow areas to dry conditions and the green areas to intermediate soil moistures. The sequence of soil moisture maps clearly shows the drying occurring during the eight days, i.e. the color of the soil moisture map is changing towards the yellows. The scatter plot is a comparison between the *in-situ* measurements and the estimated values of soil moisture over the AGO02 field. If the algorithm was perfect, tile points would fall on the diagonal dashed line. The RMS error of the soil moisture estimate is 1.696. It is noteworthy that the top of the soil moisture maps have a band where the soil moisture is significantly greater than in the rest of the image. It corresponds to an area for which the incidence angle is less than 30° and where the inversion is not working optimally.

In Figure 6, the RMS height maps corresponding to the six datatakes described in the preceding paragraph are displayed. As expected, the 6 maps are similar and indicate no trend in roughness changes. The scatter plot shows a good agreement between measured and estimated RMS heights with an RMS error of 0.15 cm. In the right part of the top half image of the June 18 roughness map, a rough (red) rectangular field is clearly visible. This field appears smooth (blue) on the five preceding dates and it is suspected that this field was plowed between June 16 and June 18.

Washita'94 was an aircraft and shuttle experiment that occurred between April 9 and April 18 in which the shuttle took data on April 11 through 17 and the AIRSAR on April 10 and 11. Two of the sampled fields where data is already available are in the radar scene and meet the low vegetation criteria described earlier. The results from the inversion are included in Table 4 both for SIR-C and for AIRSAR. We note that AIRSAR derived soil moistures are very close to the SIR-C derived values. The measured roughness for Field 12 and Field 15 are not yet available. SIR-C acquired data again over the same area on April 15, 1992. Figure 7 displays the soil moisture map derived from the two SIR-C data sets both calibrated with the same calibration factors. Between April 10 and April 15, no rain occurred in the Chickasha area and the fields dried considerably from a 20% down to a 10 % soil moisture, Figure 7 clearly shows the drying trend between the two datasets.

The soil moisture inversion algorithm was also applied to an Al RSAR dataset acquired over Spain in the summer of 91. The data acquisition campaign was part of the

Hydrological and Atmospheric Pilot EXperiment (HAPEX) of the European project on Climate and Hydrological Interactions between vegetation, Atmosphere and Land surfaces (ECHIVAL) [32]. The ECHIVAL Field Experiment in Desertification threatened Area (EFEDA) main objective was to study the land-atmosphere-vegetation interactions in a semi-arid climate. It took place in an agricultural area west of Albacete, "La Mancha, Spain. The AIRSAR data were acquired on June 19, 1991. At the same time, a large ground truth effort was taking place in the area [33]. Three of the sampled fields are in the radar scene and meet the low vegetation criteria described earlier. The results from the inversion are included in Table 4.

Table 4 summarizes the validation study of the inversion by listing all the in-situ measurements of soil moisture and surface roughness when available compared to the SAR estimated values. Figure 9 displays the estimated soil moisture versus the measured value. The overall RMS error indicates that soil moisture can be estimated in percent within $\pm 3.5\%$.

VII. CONCLUSIONS

We presented an empirical algorithm to infer soil moisture from imaging radar data over bare surfaces using two co-polarized radar cross-section measurements. The algorithm was developed with scatterometer data, and tested with several data sets acquired with the AIRSAR system, and we also presented the first soil moisture images derived from spaceborne SIR-C SAR data. A comparison with in situ data shows that the algorithm infers soil moisture with an accuracy of better than 4 %. Best results are achieved when the surface roughness is such that $kh < 2.5$ (1 O cm RMS height for L-band) and the incidence angle is larger than 30 degrees.

We also quantified the calibration requirements of the algorithm. If soil moisture must be retrieved with an accuracy better than 4 %, the radar data must be calibrated to within 2 dB absolute and 0.5 dB relative between the two co-polarized channels; current operational multipolarization SAR systems such as AIRSAR and SIR-C routinely deliver images that meet or exceed these calibration requirements. Using an NDVI image derived from SPOT data, we showed that the algorithm can be. applied successfully to areas with NDVI up to 0.4 when using L-band data. We also presented evidence that the ratio of the cross-polarized return to the like-polarized return could be used to decide which areas the algorithm can be applied to. This will be especially useful for those data

sets where cloud cover prohibits the acquisition of visible and infrared data, and where consequently no NDVI data will be available.

The results presented in this paper demonstrates that soil moisture can be measured from space using multipolarization SAR. Although the current algorithm is only applicable to bare and sparsely vegetated areas, work is continuing to extend the algorithm to areas with more vegetation. If such a multipolarization SAR system could be placed in earth orbit, our results indicate that long- term global soil moisture monitoring can be a reality. This will provide one of the most important inputs into global climate models and could significantly improve our understanding of the Earth's changing climate.

ACKNOWLEDGMENT

We would like to thank our colleagues from University of Michigan and University of Berne for sharing their scatterometer data and the corresponding ground truth with us. Our gratitude also goes to all the people involved in collecting the ground truth we used to validate this study. This includes the organizer as well as the participants to the WASHITA campaign and the EFEDA campaign We would also like to acknowledge the help we received from Tom Jackson and his team for providing us with the NDVI map of our area of study. This work was performed at the Jet Propulsion laboratory, California Institute of Technology under contract with the National Aeronautics and Space Administration.

REFERENCES

[1] Walker, J.M and P.R. Rowntree, "The effect of soil moisture on circulation and rainfall in a tropical model," Q.J.R. Meteorol. Sot., 103, pp.29-46, 1977

[2] Delworth T. L. and S. and Manabe, " The influence of potential evaporation on the variabilities of the simulated soil wetness and climate," J. Climate, 1(5), pp523-547, 1988

[3] Fast, J.D. and M.D. McCorcle, "The effect of heterogeneous soil moisture on a summer baroclinic circulation in the central United States," Monthly Weather Review, vol. 119, 1991

[4] Chang, J.T. and P.J. Wetzel, 'Effects of spatial variations of soil moisture and vegetation on the evolution of a prestorm environment: a numerical case study, " Monthly Weather Review, vol. 119, 1991.

[5] Lanicci, J.M, T.N. Carlson and T.T. Warner, "sensitivity of the Great Plains sever-storm environment to soil moisture distribution, " Monthly Weather Review, vol.1 15, 1987.

[6] Betts, A.K., J.H Ball, A.C. Baljaars, M.J. Miller and P. Viterbo,' Coupling between land surface, boundary layer parametrizations and rainfall on local and regional scales: Lessons from the wet summer of 1993," Fifth conference on Global Change Studies: American Meteor. Sot., 74th Annual Meeting, Nashville, Term., Jan23-28, 1994.

[7] Engman, E. T., "Applications of Microwave Remote Sensing of Soil Moisture for Water Resources and Agriculture, " Remote Sensing of the Environment, vol. 35, 1991, pp 213-226.

[8] Wang, J. R., E.T. Engman, J.C Shiue, M. Rusek and C. Steinmeier, "The SIR-B observations of microwave dependence on soil moisture, surface roughness, and vegetation covers, " IEEE Trans. on GRS, vol. GE-24, No 4, Apr 1986.

[9] Evans, D.L. , T.G. Farr, J.J. vanZyl, " Estimates of Surface Roughness Derived from Synthetic Aperture Radar (SAR) data". IEEE Trans. on GRS, vol.30, N02, March 1992.

[10] Oh, Y., K. Sarabandi, F.T. Ulaby, "An Empirical Model and an inversion Technique for Radar Scattering from Bare Soil Surfaces," IEEE Trans. Geosc. Remote Sensing, vol. GE-30, 1992, pp 370-381,

[11 Tassoudji, M. A., K. Sarabandi, F. T. Ulaby, "Design Consideration and implementation of the LCX Polarimetric Scatterometer (POLARSCAT), " Rep 022486-T-2, Radiation Laboratory the University of Michigan, June 1989.

[12] Wegmuller, U., "Active and Passive Microwave Signature Catalogue on Bare Soil (2-12 GHz), " institute of Applied Physics, University of Berne, Switzerland, 1993.

[13: Brunfeldt, D. R., "Theory and Design of a field portable dielectric measurement system," IEEE Int. Geosci. Remote Sensing S yn ıp. (IGARSS) Digest, vol. 1, pp559-563, 1987.

[14 Hallikainen, M.T., F. T. Ulaby, M. C. Dobson, M.A. El-Rayes and L. Wu, " Microwave dielectric behavior of wet soil - Part I: Empirical models and experimental observations," IEEE Trans. Geosc. Remote Sensing, vol. GE-23, pp 25-34, 1985.

[15] Huppi R.: Dissertation, Institut fur Angewandte Physik, Universitat Bern, 1987

[16] Blanchard, B. J., A.T.C. Chang, "Estimation of soil moisture from SEASAT SAR data ," Water Resources Bulletin, American Water Resources Association, Vol. 19, No. 5, October 1983.

[17] Dubois, P.C, E. Rignot, J.J. van Zyl, "Direction angle sensitivity of agricultural field backscatter with AIRSAR data," IEEE Int. Geosci. Remote Sensing Symp. (IGARSS) Digest, vol. 2, pp1680-1682, 1992.

[18] Wegmuller, U., Lizentiatsarbeit, Institut fur Angewandte Physik, Universitat Bern, 1986.

[19] Ulaby, F. T., R. K. Moore, and A. K, Fung, Microwave Remote Sensing: Active and Passive, 3, From theory to Applications, pp. 1065-2162, Dedham, MA: Artech House, *1986*

[20] van Zyl,J, " Calibration of polarimetric radar images using onl y image parameters and trihedral corner reflector responses", IEEE Transactions on Geoscience and Remote Sensing, vol. 28, No.3, pp337-348, May 1990

[21] Le Toan,T., A. Beaudoin and D. Guyon, " Relating forest biomass to SAR data," IEEE Transactions on Geoscience and Remote Sensing, Vol. 30, No. 2, March 1992.

[22] Durden, S.L. ,J.J van Zyl and H.A. Zebker, " Modeling and observation of the radar polarization signature of forested areas," IEEE transactions on Geoscience and Remote Sensing, Vol. 27, No.3, May 1989.

[23] Tucker, C. J., "Red and photographic infrared combinations for monitoring vegetation," Remote Sensing of the Environment, 8:127-1 SO, 1979

[24] Tucker, C. J., "A critical review of remote sensing and other methods for estimation of standing crop biomass," Grass Forage Science, 35.177-182, 1980

[25] van Zyl, J., R. Carande, Y. Lou, T. Miller and K, Wheeler, "The NASA/JPL three-frequency polarimetric AIRSAR system", IEEE Int. Geosci. Remote Sensing Symp. (IGARSS) Digest, vol. 1, pp 649-651,1992,

[26] Cruz, J., A. Freeman, "Calibration and image quality results of the NASA/JPL aircraft SAR for the J-ers 1 Calibration campaign", JPL internal document, D-9345, January 92.

[27] Freeman, A., Y. Shen, J. van Zyl and J.D. Klein, "Calibration of NASA/JPL DC-8 SAR data,", IEEE Int. Geosci. Remote Sensing Symp. (IGARSS) Digest, vol. 3, pp1377-1 379, 1991

[28] Dubois, P., D. Evans and J. van Zyl, "Approach to derivation of SIR-C science requirements for calibration", IEEE Transactions on Geoscience and Remote Sensing, vol. 30, No6,ppl145-1149, Nov. 1992.

[29] T.J. Jackson, F.R. Shiebe (cd.), "Washita'92 data report ," NAWQL Report 101, USDA National Agricultural Water Quality Lab, Durant OK, 1993

[30] Evans, D. L., J.J. van Zyl and C.F. Burnette, " Incorporation of polarimetric radar images into multi-sensor data sets,'" IEEE Transactions of Geoscience and Remote Sensing, GE-28, pp.932-939, 1990

[31] Dubois P.C, E. Rignot, M. Borgeaud, F. Burnette, S. Okonek and J.J van Zyl, " SAR-REG - Registration-Tie pointing software for SAR data," Available through COSMIC, NPO-19380, 1994.

[32] Belle, H. J. and B. Streckenbacb, " The ECHIVAL field experiment in a desertification-threatened area EFEDA, " First Annual Report to EC, published by the EFEDA-secretariat, Free University of Berlin, Berlin, Germany, 1992

[33 Bastiaanssen, W. G. M., D.H. Hoelman and R.A. Rebelling, "A Methodology for the assessment of surface resistance and soil water storage variability at mesoscale based on remote sensing measurements: A case study with HAPEX-EFEDA data, " UNESCO- International Hydrological Program 1 V, Rapport 38, ISSN 0926-230X, Vakgroep Waterhuishouding, Wageningen, July 1993

LIST OF TABLES AND FIGURES:

radar estimated surface RMS heights and in-situ measurements over the AG002 site outlined in the black and white image. Chickasha AG002 site, located to the east of Chickasha, Oklahoma,

Figure 7: L-Band HH image and two soil moisture maps derived from SIR-C data for April 12, 94 and April 15,94. The first day was extremely wet and the second day was drier.

Figure 8: Radar estimated soil moisture versus measured soil moisture for the different active microwave data sets where both radar data and in-situ soil moisture measurements were available. The overall RMS error is 3.5%.

Surface	RMS Height h (cm)	μ_v	kh (1.5 GHz)	kh (4.75 GHz)	kh (9.5 GHz)
S_1	0.4	0.31	0.13	0.40	0.80
S_1	0.4	0,19	0.13	0.40	0.80
S_2	0.32	0.29	0.1	0.32	0.64
S_2	0.32	0.14	0.1	0.32	0.64
S3	1.12	0.31	0.35	1.11	2.23
S3	1.12	0.19	0.35	1.11	2.23
S4	3.02	0.20	0.95	3.00	6.01
S_4	3.02	0.17	0.95	3.00	6.01

Table 1

Field ID	RMS Height h (cm)	μ_v	kh (2.5 GHz)	kh (11.0 GHz)
4	1.	0,17	0.52	2.32
6	0.57	0.28	0.30	1.33
7	0.69	0.21	0.36	1.61
30	1,12	0.22	0.59	2.61
31	1,06	0,20	0.56	2.47
32	0.77	0.18	0.40	1.79
33	1.06	0.18	0.56	2.47
39	1.06	0.22	0.56	2.47

Table 2

Absolute/Relative	C-Band	L-Band	P-band
AIRSAR	±1.0 dB/ ±0.4 dB	±1.2 dB/ ±0.5 dB	±1.9 dB/ ±1.3 dB
SIR-C	±2.0 dB/ ±0.4 dB	±2.0 dB/ ±0.4 dB	NA

Table 3

Table4

Scene	Sensor	Data Take	Date	Field ID	Mv Measured ['?40]	Mv Estimated [%]	h Measured (cm)	h Estimated (cm)
CHICKASHA	AIRSAR	3902	6/1 0/92	AGO02	28.7	29.2	1.19	1.18
CHICKASHA	AIRSAR	3664	6/1 2192	AGO02	22.4	21.15	1.19	1.35
CHICKASHA	AIRSAR	3359	6/1 3192	AGO02	24.1	23.5	1.19	1.09
CHICKASHA	AIRSAR	3875	6/14/92	AGO02	18.1	19.4	1.19	1.19
CHICKASHA	AIRSAR	3883	6/1 6/92	AGO02	13.6	16.95	1.19	1.24
CHICKASHA	AIRSAR	3360	6118192	AGO02	11.6	12.1	1.19	1.45
CHICKASHA	AIRSAR	4040	6/17/92	AGO02	17.5	18.5	1.19	1.45
CHICKASHA	AIRSAR	4041	6/13/92	AGO02	24.1	27.4	1.19	1.38
CHICKASHA	AIRSAR	Mosaic	6/1 3/92	RG148	27.6	30.6		
CHICKASHA	AIRSAR	Mosaic	6/1 3/92	RG131	29.2	34.5		
CHICKASHA	AIRSAR	4254	4/12/94	Field 12	18.4	24.5		1.58
CHICKASHA	AIRSAR	4254	4/12/94	Field 15	24.8	21.8		0.86
EFEDA	AIRSAR	3146	6113190	Field 2	3.4	6.9	1.41	1.34
EFEDA	AIRSAR	3146	6/13190	Field 4	30.6	22.8	0.6	0.9
EFEDA	AIRSAR	3146	6113190	Field 5	18.6	18.2	1.79	0.8
CHICKASHA	SIR-C	10155	4/12/94	Field 12	18.4	20.2		1.2
CHICKASHA	SIR-C	10155	4/12/94	Field 15	24.8	30.3		1.24
CHICKASHA	SIR-C	10158	4/15/94	Field 12	9.9	12.5		2
CHICKASHA	SIR-C	10158	4/15/94	Field 15	12.5	11.8		1.5
RMS ERROR						3.32039154/		0.34172025

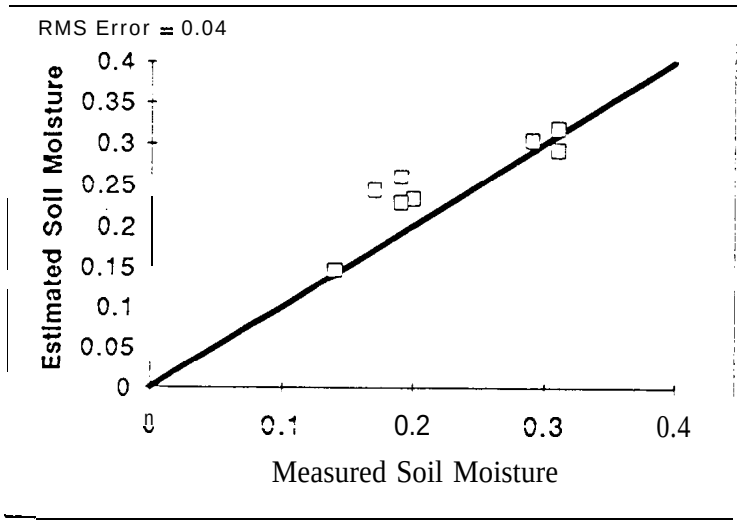
RMS Error = 0.04
Estimated Soil Moisture
0.4
0.35
0.3
0.25
0.2
0.15
0.1
0.05
0
0
0.1
0.2
0.3
0.4
Measured Soil Moisture

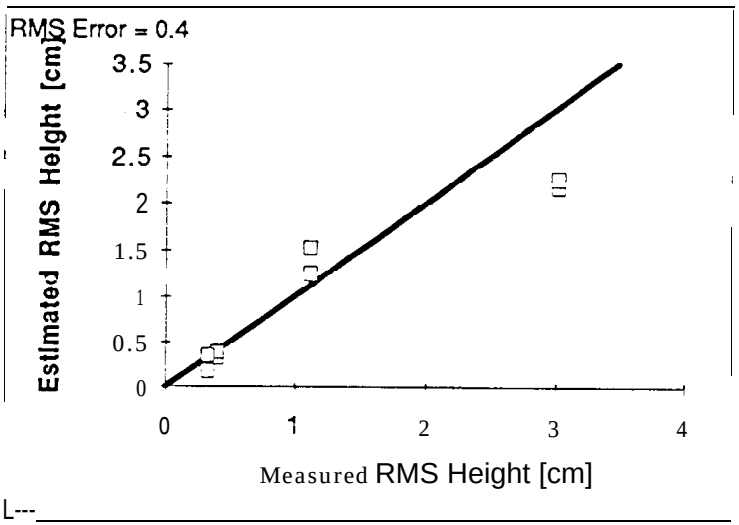
RMS Error = 0.4
Estimated RMS Height [cm]
3.5
3
2.5
2
1.5
1
0.5
0
0
1
2
3
4
Measured RMS Height [cm]

FIGURE 1

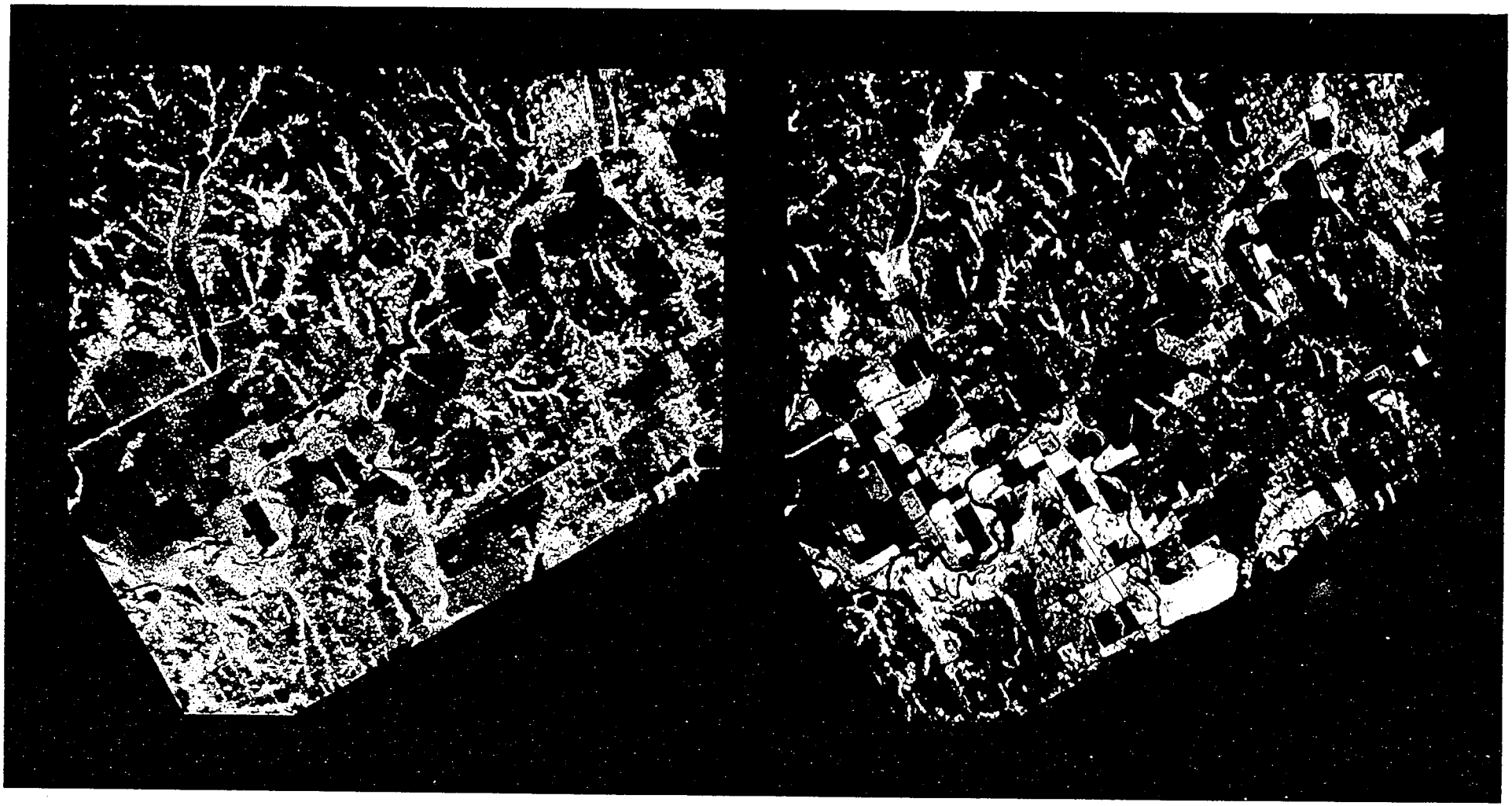

(a)

(b)

FIGURE 2

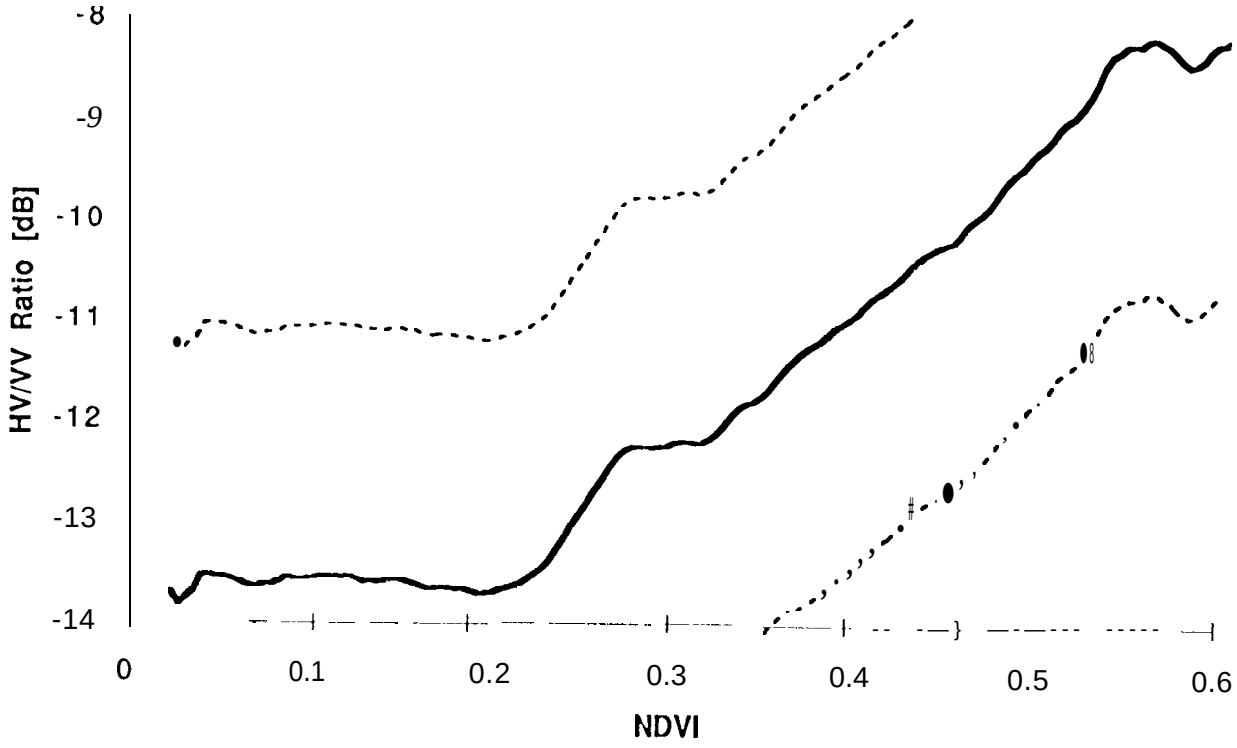

Figure 3

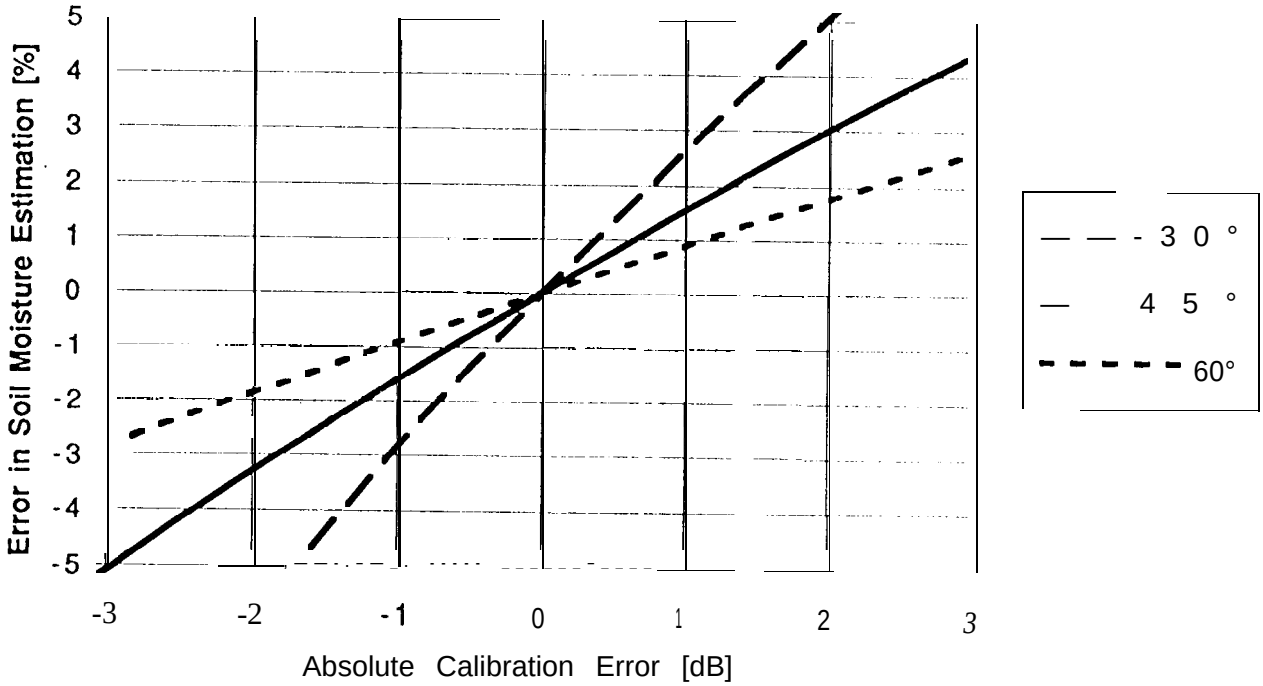
Error in Soil Moisture Estimation [%]
5
4
3
2
1
0
-1
-2
-3
-4
-5
-3
-2
-1
0
1
2
3
Absolute Calibration Error [dB]
30°
45°
60°

Figure 4a

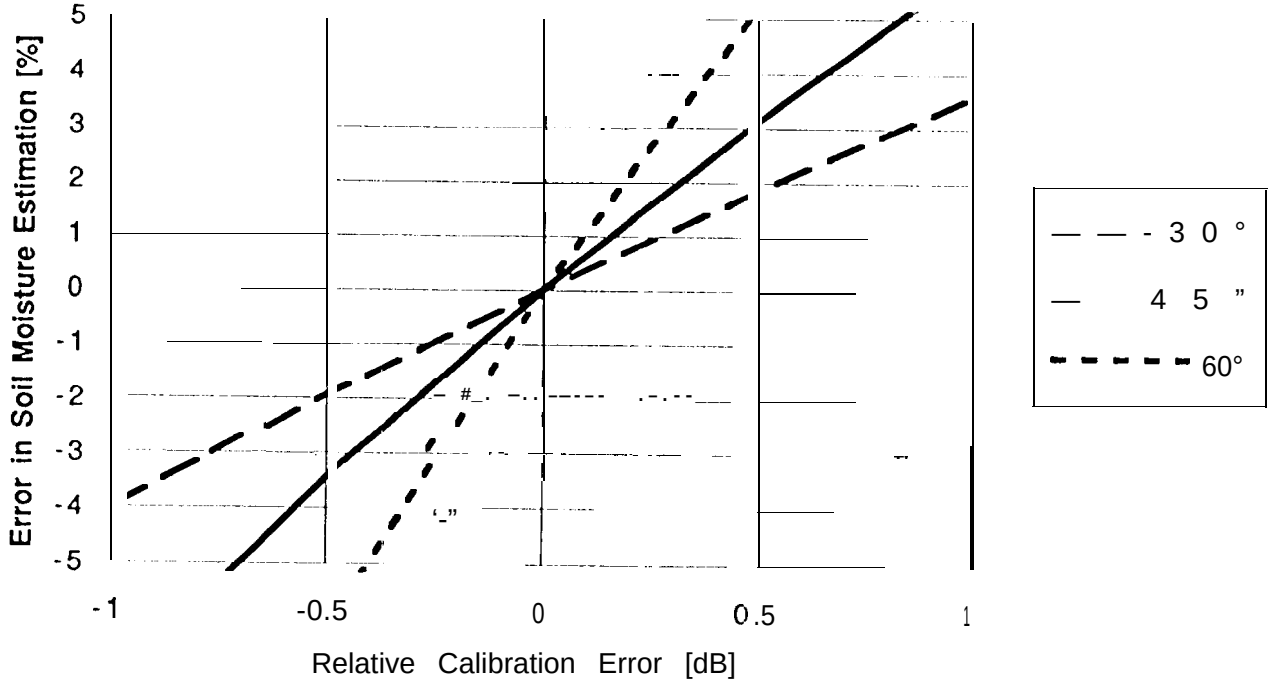
Error in Soil Moisture Estimation [%]
5
4
3
2
1
0
-1
-2
-3
-4
-5
-1
-0.5
0
0.5
1
Relative Calibration Error [dB]
30°
45°
60°

Figure 4b

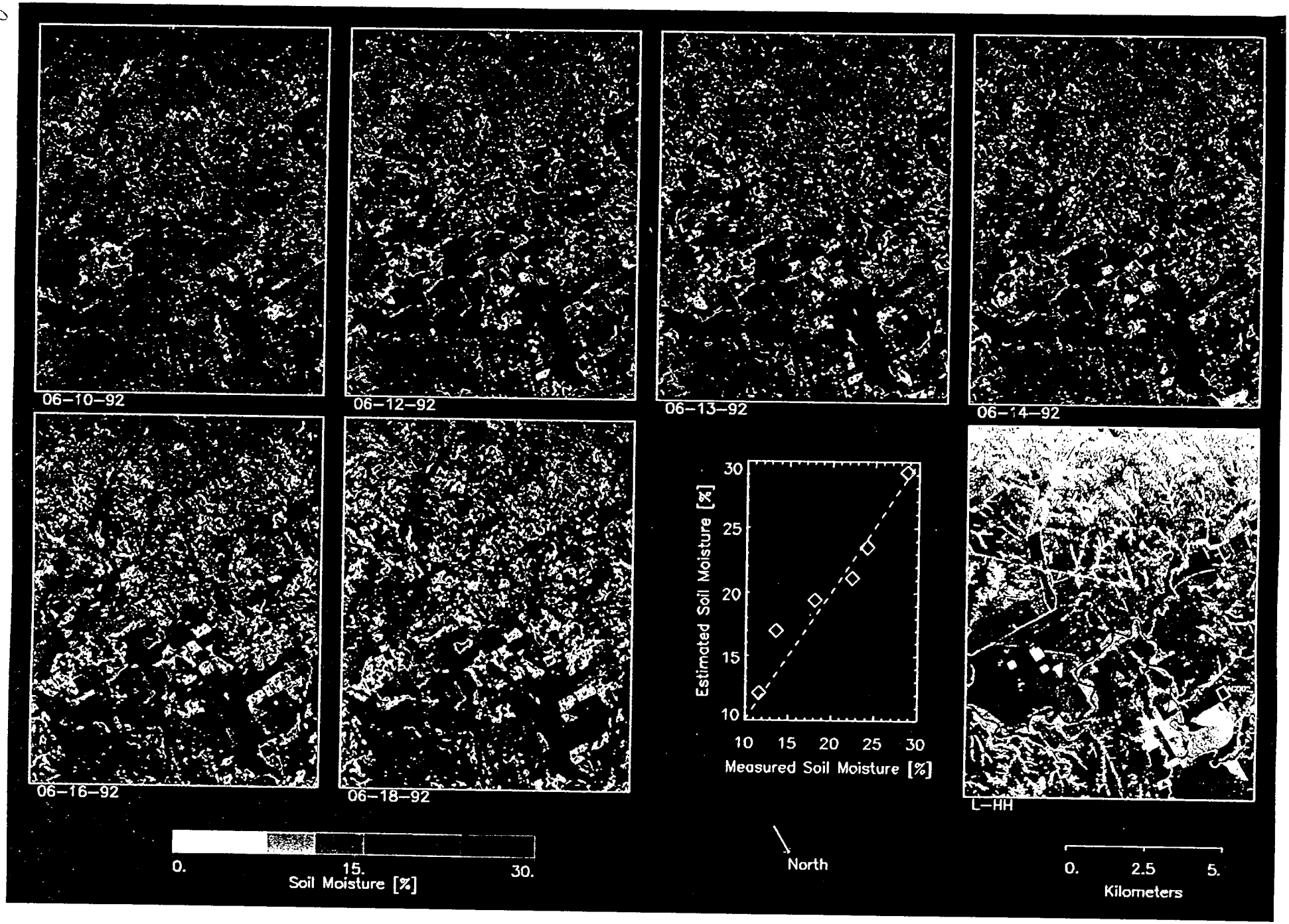
06-10-92
06-12-92
06-13-92
06-14-92
06-16-92
06-18-92
Estimated Soil Moisture [%]
Measured Soil Moisture [%]
10
15
20
25
30
L-HH
0.
15.
30.
Soil Moisture [%]
North
0.
2.5
5.
Kilometers

Figure 5

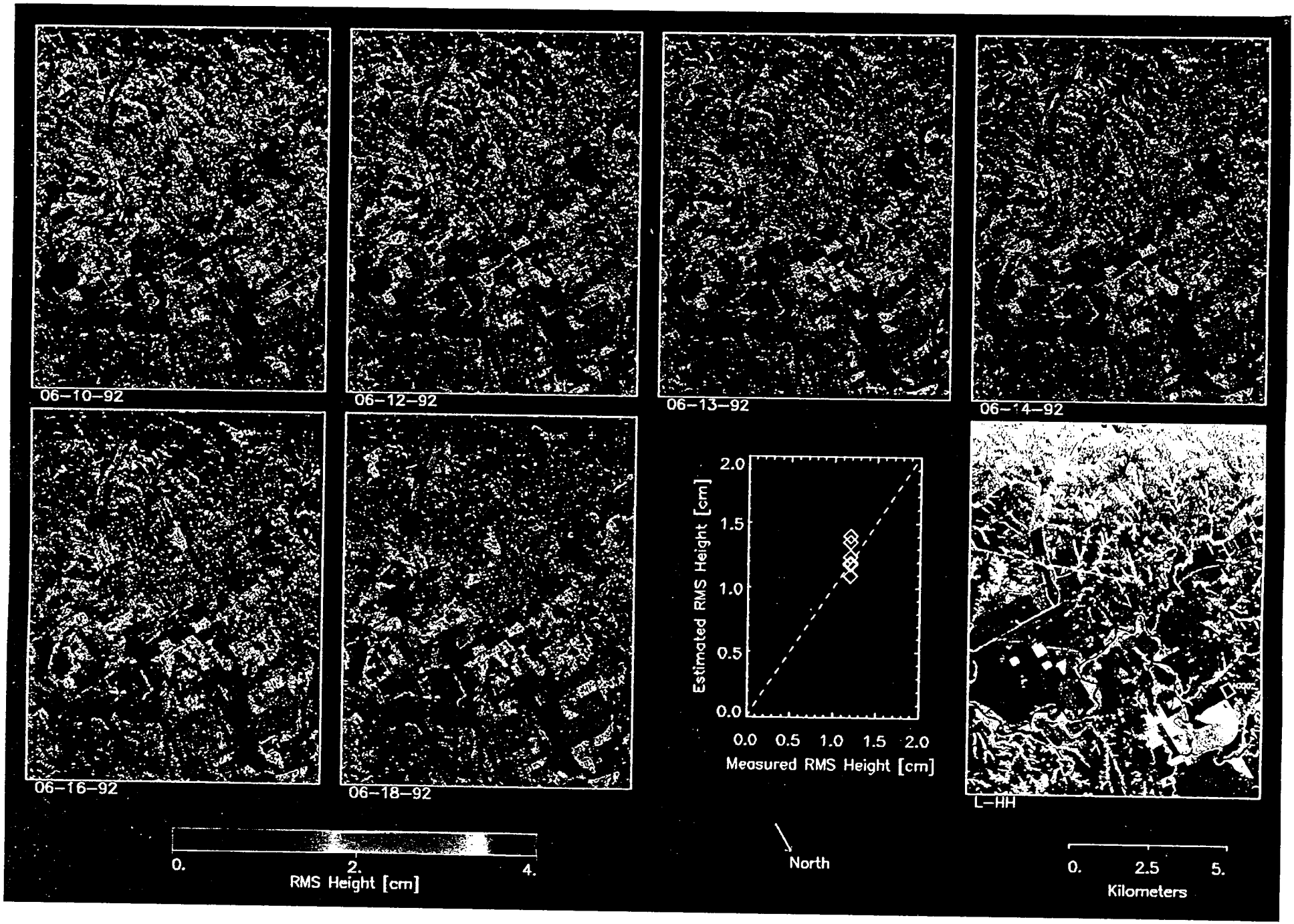
06-10-92
06-12-92
06-13-92
06-14-92
06-16-92
06-18-92
Estimated RMS Height [cm]
2.0
1.5
1.0
0.5
0.0
0.0 0.5 1.0 1.5 2.0
Measured RMS Height [cm]
L-HH
0. 2. 4.
RMS Height [cm]
North
0. 2.5 5.
Kilometers

FIGURE 6

SIR C
CHICKASHA, OKLAHOMA

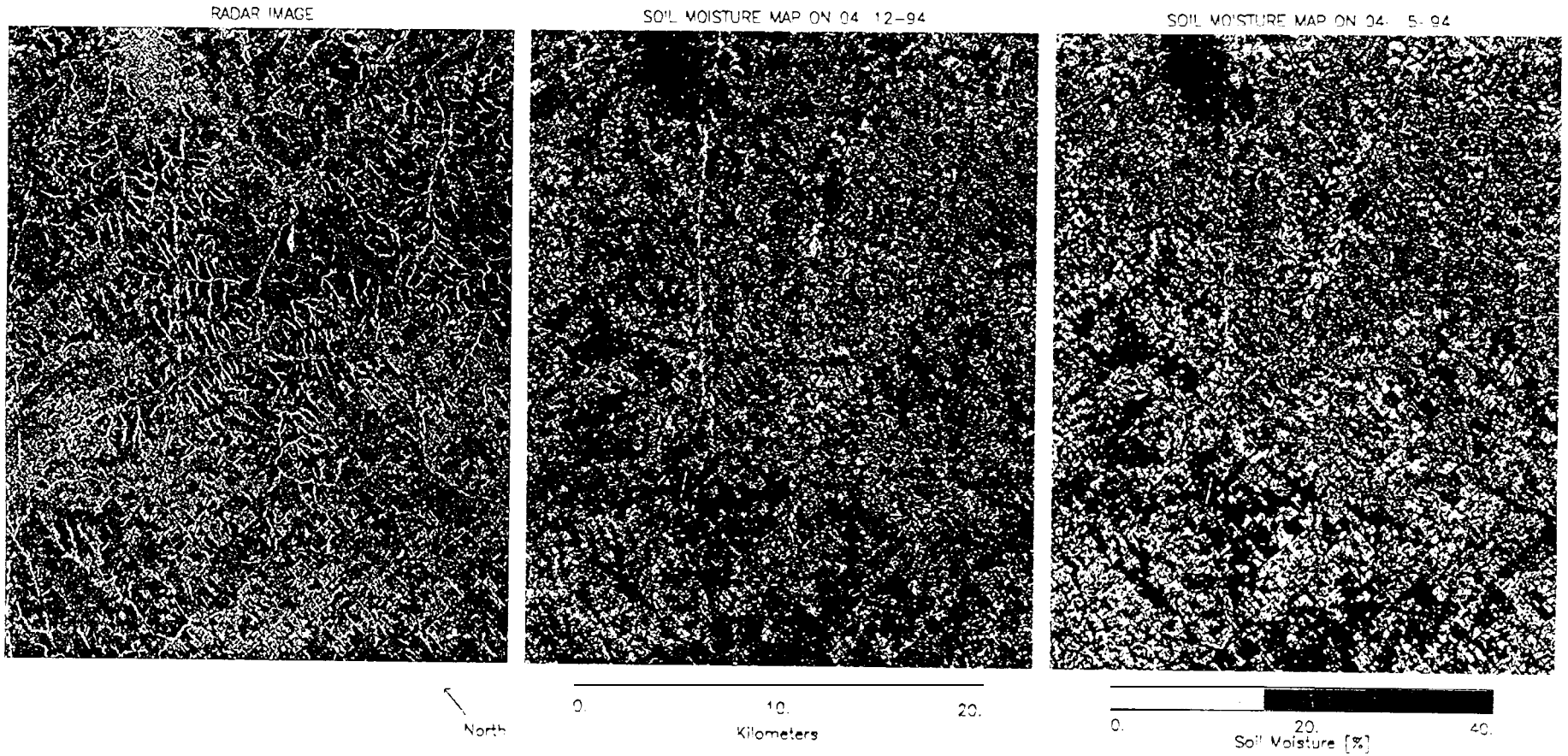

FIGURE 7

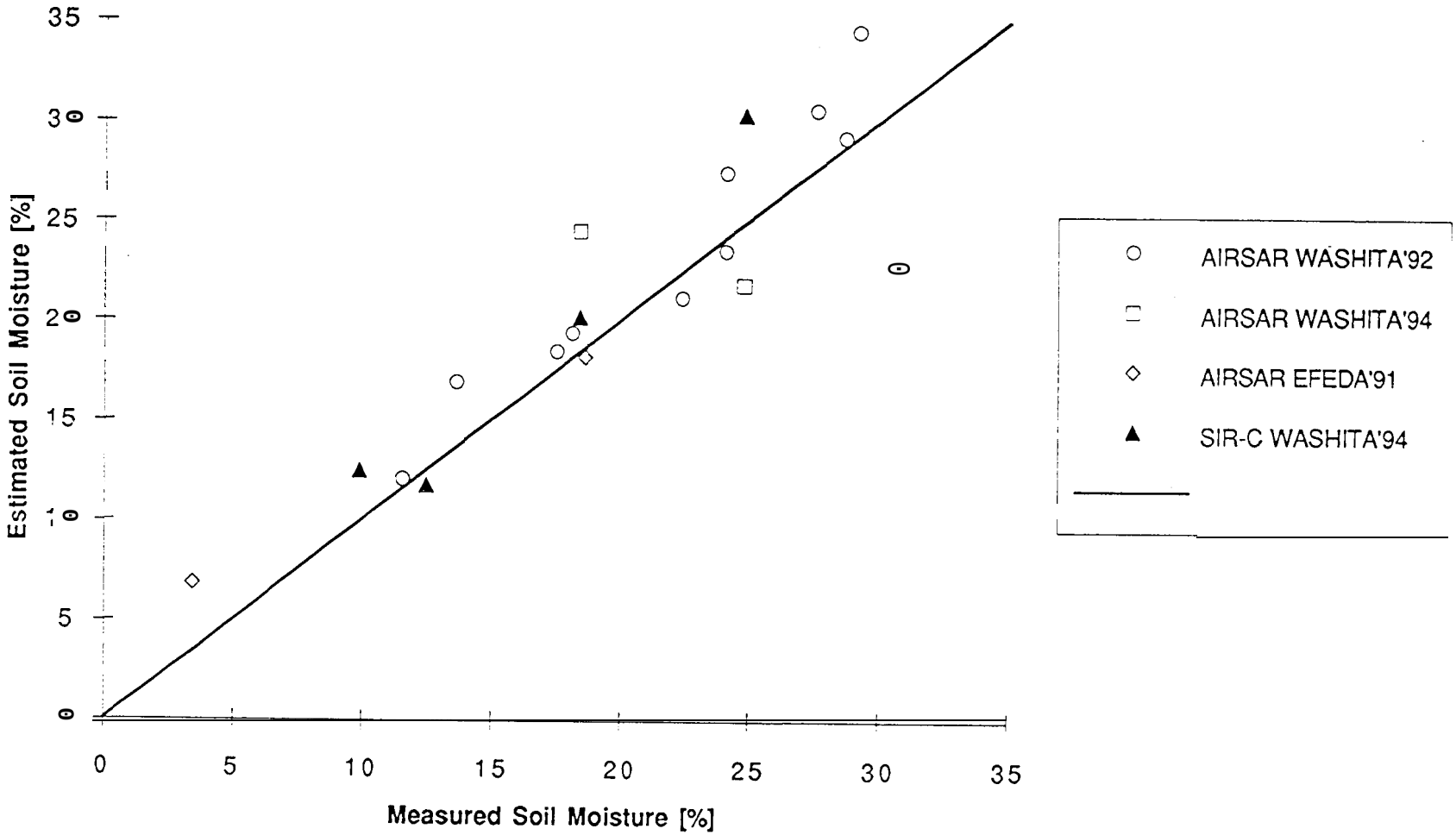
Estimated Soil Moisture [%]
Measured Soil Moisture [%]
0
5
10
15
20
25
30
35
AIRSAR WASHITA'92
AIRSAR WASHITA'94
AIRSAR EFEDA'91
SIR-C WASHITA'94

Figure 8